PCCP

Accepted Manuscript

ROYAL SOCIETY OF CHEMISTRY

www.rsc.org/pccp

Generalized Approximate Spin Projection Calculations of Effective Exchange Integrals of the $CaMn_4O_5$ Cluster in the S_1 and S_3 States of Oxygen Evolving Complex of Photosystem II

H. Isobe[a], M. Shoji[b], S. Yamanaka[c], H. Mino,[d] Y. Umena[e], K. Kawakami[e], N. Kamiya[e], J.-R. Shen[a] , and K. Yamaguchi[f,g]*

[a]Graduate School of Natural Science and Technology, Okayama University, Okayama 700-8530, Japan

[b]Center of Computational Sciences, Tsukuba University, Tsukuba, Ibaraki 305- 8577, Japan

[c]Graduate School of Science, Osaka University, Toyonaka, 560-0043, Japan

[d]Division of Material Science (Physics), Graduate School of Science, Nagoya University, Furo-cho, Chikusa, Nagoya, 464-8602, Japan

[e]The OCU Advanced Research Institute for Natural Science and Technology (OCARNA), Osaka City University, 3-3-138 Sugimoto, Sumiyoshi, Osaka 558-8585, Japan

[f]Handai Rigaku Techno-Research, Toyonaka, Osaka 560-0043, Japan

[g]Institute for NanoScience Design, Osaka University, Toyonaka, Osaka, 560-0043, Japan

Abstract

Full geometry optimizations followed by the vibrational analysis were performed for eight spin configurations of the $CaMn_4O_4X(H_2O)_3Y$(X=O, OH; Y=H_2O, OH) cluster in the S_1 and S_3 states of oxygen evolution complex (OEC) of photosystem II (PSII). The energy gaps among these configurations obtained by vertical, adiabatic and adiabatic plus zero-point-energy (ZPE) correction procedures have been used for computation of the effective exchange integrals (J) in the spin Hamiltonian model. The J values are calculated by (1) analytical method and (2) generalized approximate spin projection (AP) method that eliminates the spin contamination errors of UB3LYP solutions. Using J values derived from these methods, exact diagonalization of the spin Hamiltonian matrix was carried out, yielding excitation energies and spin densities of the ground and lower-excited states of the cluster. The resulted results for the right (R)- and left (L)-opened structures in the S_1 and S_3 states are found to be consistent with available optical and magnetic experimental results. Implications of the computational

results are discussed in relation to a) the necessity of the exact diagonalization for computations of reliable energy levels, b) magneto-structural correlations in the $CaMn_4O_5$ cluster of OEC of PSII, c) structural symmetry breaking in the S_1 and S_3 states, and d) the right- and left-handed scenarios for the O-O bond formation for water oxidation.

I. Introduction

Past decades a number of electron paramagnetic resonance (EPR) experiments have been performed to elucidate electronic structure and function of the catalytic site for water oxidation in oxygen evolving complex (OEC) of photosystem II (PSII).[1-40] In early 1980th Dismukes and Siderer[1] have first reported the EPR spectrum in the S_2 state of the Kok cycle for water oxidation. The EPR spectrum obtained is consistent with a tetramer of Mn ions, in which Mn(III) and Mn(IV) oxidation states are present. The S_2 state of PSII exhibits two distinct classes of EPR signals; [1-19] (a) ^{55}Mn (I=5/2) hyperfine-resolved signal centered near g=2 for the doublet state (S=1/2) and (b) broader signal without hyperfine structure centered near g=4.1 for the S=5/2 spin state. The broken-symmetry (BS) density function theory (DFT) computations[41-43] have revealed that the right (R)-opened structure, $Mn(IV)_{4(a)}$-$O_{(5)}$….$Mn(III)_{1(d)}$, of the $CaMn_4O_5$ cluster is responsible for the multi-line g=2 doublet state (S=1/2) spectra, whereas the left (L)-opened structure, $Mn(III)_{4(a)}$….$O_{(5)}$ –$Mn(IV)_{1(d)}$, of the cluster is consistent with the g=4.1 sextet spin state (S=5/2) spectra.[41-43] Boussac et al[14-16] have shown that the spin crossover between the R(S=1/2) and L(S=5/2) configurations has been induced by the near-infrared light (NIR) illumination. EPR[1-19] and BS DFT[41-43] studies have elucidated the magneto-structural correlations in the S_2 state of OEC of PSII.

Dexheimer and Klein[20] have reported the parallel polarization EPR signal that is consistent with the paramagnetic spin (S=1) state of the S_1 state of OEC of PSII, suggesting that the triplet state (S=1) corresponds to the reduced form of the $CaMn_4O_5$ cluster with the multiline g=2 doublet state (S=1/2) spectra. Koulogliotis et al[21] have performed the EPR studies of the S_1 state, concluding that the ground spin state of the S_1 resting state is diamagnetic, whereas the S_1 active state is paramagnetic. Yamauchi et al[22] have also performed the parallel polarization EPR studies of the S_1 state followed by the temperature variation experiment, elucidating that the signal at g=4.8 originates from an excited state with triplet spin state (S=1) with separation from the diamagnetic ground state (S=0) of about 2. 5 K (1.74 cm^{-1}). They have shown that the S=1 signal is

not detected for the methanol-treated OEC of PSII, although the illumination of the sample provides the normal multiline S_2 signal. Campbell et al[23] have observed an alternative multiline signal at g=12 for the S_1 state with the $Mn(III)_2Mn(IV)_2$ oxidation state. Thus accumulated EPR results[20-23] have suggested the existence of EPR active and inactive species in the S_1 state.

Matsukawa et al[24] have observed the parallel polarization EPR signals at g=12 and 8 for the S_3 state of OEC of PSII. Successful simulations have shown that the signals can be assigned to the perpendicular and parallel components relative to the magnetic field direction. Temperature dependence of the signal intensity has revealed that the signals arise from a low-lying triplet (S=1) excited state. Ioannidia and Petrouleas[25] have confirmed the same EPR signals, together with a g=4 signal for the S_3 state. They have shown that the signals vanish in the presence of methanol. Boussac et al[26] have revealed complete EPR spectrum for the S_3 state involving g=8 and g=4 signals. Simulations of the spectrum have indicated that the S_3 experimental EPR spectrum is associated with a pure sextuplet (S=3) spin system and not with a triplet (S=1) state.[24] Boussac et al[26] have pointed out that the S=3 state observed indicates a coupling of all the oxidized species: a direct consequence is that the oxidation occurs at either a Mn(III) ion or ligand in the coordination sphere of the $CaMn_4O_5$ cluster. Accumulated EPR results[24-26] also suggested the existence of EPR active and inactive species in the S_3 state.

The accumulated EPR results[1-40] for the S_1 and S_3 states in OEC provide the experimental foundations for elucidation of the magneto-structural correlations in these states on the basis of the broken-symmetry (BS) density functional theory (DFT) calculations starting from the high-resolution XRD structure at 1.9 Å resolution for the S_1 state.[44-51] To this end, the energy gaps among eight spin configurations[42] for the $CaMn_4O_4X(H_2O)_3Y$(X=O, OH; Y=H_2O, OH) cluster in the S_1 and S_3 state have been obtained by three different methods: a) vertical approximation where the fully optimized geometry of the highest spin (HS) configuration is assumed for other seven configurations; b) adiabatic approximation where full geometry optimizations of eight spin configurations are performed; and c) adiabatic plus zero-point-energy (ZPE) correction approximation. By using the generalized approximate spin projection (GAP) method[52-54] that eliminates spin contamination error in BS DFT computations, the energy gaps have been mapped into the effective exchange integrals (J) in the Heisenberg spin Hamiltonian model for the $CaMn_4O_5$ cluster of OEC of PSII. Analytical expressions of the J values are also derived for lucid understanding of the mapping procedures. The exact diagonalization of the spin Hamiltonian model has

been performed to elucidate energy levels and spin densities for the ground and lower-lying excited states of the right (R)- and left (L)-opened structures. Implications of present computational results are discussed in relation to a) the necessity of the exact diagonalization for computations of reliable energy levels, b) magneto-structural correlations in the $CaMn_4O_5$ cluster of OEC of PSII, c) structural symmetry breaking in the S_1 and S_3 states, and d) the right- and left-handed scenarios for the O-O bond formation for water oxidation.

II. Computational procedures

II. 1 Geometry optimizations

Past several years the degree of symmetry breaking of the Mn_a-X-Mn_d bond ($X=O_{(5)}$) in the $CaMn_4O_5$ cluster has been under great debates[41-43,51, 52,56-67] because the high-resolution XRD structure[44] has revealed almost symmetrical structure. Our previous BS DFT computations[42,43] starting from the XRD geometry[44] have revealed that the structural symmetry breaking (SSB) via the Jahn-Teller effects of Mn(III) ions is a key concept for theoretical understanding of possible geometries of the $CaMn_4O_4X(H_2O)_4Y$ (X=O or OH; Y= H_2O or OH) cluster, and have revealed three possible geometrical structures: right-opened (R; Mn_a-X….Mn_d), central (C; Mn_a-X-Mn_d) and left-opened (Mn_a….X-Mn_d) ones. However, the structural symmetry breaking (SSB) in the S_1 and S_3 states have been investigated by geometry optimizations based on the high-spin (HS) solution.[42] We here perform full geometry optimizations of all the spin configurations to elucidate energy levels and relative stabilities for these configurations in the S_1-and S_3-states. Figure 1 illustrates possible cluster structures examined in this paper: (A) $\mathbf{S_{1a}}$(R) (X=O;Y= H_2O), $\mathbf{S_{1b}}$(C) (X=Y=OH), $\mathbf{S_{3a}}$(R)-H_2O (X=O, Y= H_2O, W=OH) and $\mathbf{S_{3a}}$(L) (X=O, Y= H_2O,W= OH), structures, where the notations ‘’a’ and ‘b’ represent X=O and X=OH, respectively. Tables S1 and S2 summarize the optimized geometrical parameters for $\mathbf{S_{1a}}$(R) and $\mathbf{S_{1b}}$(C) structures, respectively. Tables S3 and S4 summarize the optimized geometrical parameters for $\mathbf{S_{3a}}$(R)-H_2O and $\mathbf{S_{3a}}$(L)-H_2O structures, respectively.

Figure 1

II. 2 Heisenberg spin Hamiltonian model for four site systems

The approximate spin projection (AP) scheme[55] has been generalized for multi-nuclear complexes, affording a generalized AP (GAP) scheme[53,54] that has been applied for the $CaMn_4O_4X(H_2O)_4Y$ cluster.[45-52] Six effective exchange integrals (J) for the systems are determined by using the energy gaps among the eight spin configurations (Fig. 2) obtained by the vertical, adiabatic and adiabatic plus ZPE methods. Analytical expressions and theoretical explanations of the effective exchange

integrals (J) in the S_1 and S_3 states are also shown in supporting material SIII. The exact diagonalization of the spin Hamiltonian matrix consisted of the calculated J values has been performed to elucidate excitation energies and spin densities. All the BS DFT computations[68-70] have been performed using Gaussian09 (G09) program.[71]

The basis sets, LANL2DZ for Mn and Ca atoms and 6-31D(d) for C, H, O and N atoms, which are referred to as basis set I, are used for geometry optimizations.[68-71] Frequency calculations have been carried out with the basis set I to verify the nature of all stationary points and to derive zero-point energies (ZPE) without scaling and thermodynamics effects at 298.15 K.[42] In this paper relative stabilities among the eight spin configurations and J values are obtained by using the basis set I since full geometry optimizations of all the spin configurations at the ultra fine convergent conditions by the more flexible basis set II[42] are too heavy to obtain J values under the adiabatic plus ZPE approximation.

III Computational results for the S_1 state

III. 1 The optimized geometrical parameters of eight spin configurations

The total high-spin (HS) (↑↑↑↑) UB3LYP solution (Fig. S2A),[42] has first been employed for full geometry optimization of the $CaMn_4O_4X(H_2O)_4Y$ cluster. Starting from the optimized geometrical structure of HS, full geometry optimizations of the remaining seven configurations have been performed. The zero point energy (ZPE) corrections have also been obtained by the frequency analysis for each optimized structures. These are referred to as the 'adiabatic' and the 'adiabatic plus ZPE correction' methods. From Table S1, the optimized geometrical parameters for the right-opened S_1 structure $\mathbf{S_{1a}}$(R) (X=O;Y=H_2O) are almost the same among the eight-different spin configurations. The optimized Mn-Mn distances for $\mathbf{S_{1a}}$(R) indicate a general trend, named the rule 'Ib': $R(Mn_a\text{-}Mn_b) < R(Mn_b\text{-}Mn_c) \sim R(Mn_c\text{-}Mn_d) < R(Mn_b\text{-}Mn_d) < R(Mn_a\text{-}Mn_d)$. The trend 'Ib' is common for the right(R)-opened structure under the assumption that the $O_{(5)}$ site is an oxygen dianion.

The optimized geometrical parameters for the proton-shifted structure $\mathbf{S_{1b}}$(C) (X=Y=OH) are almost the same among the eight-different spin configurations as shown in Table S2. Subtle geometry changes are however responsible for variations of effective exchange integrals as discussed in later sections. The average Mn-Mn distances for $\mathbf{S_{1b}}$(C) exhibits the general trend, named rule 'Ia'[42]: $R(Mn_b\text{-}Mn_c) \sim R(Mn_c\text{-}Mn_d) < R(Mn_a\text{-}Mn_b) < R(Mn_b\text{-}Mn_d) < R(Mn_a\text{-}Mn_d)$. The rule Ia is consistent with the high-resolution XRD structure at 1.9 Å resolution.[44] The $Mn_a\text{-}Mn_b$ distance is elongated with protonation of the oxygen dianion at the X-site; $X=O_{(5)}H$. Details of the optimized geometrical parameters are given in supporting material (SI).

III.2 Relative stabilities of the eight spin configurations by UB3LYP

Table S5 summarizes relative energies of the eight spin configurations for the right-opened structure $\mathbf{S_{1a}}$(R)(X=O;Y=H_2O) on the basis of the vertical, adiabatic and adiabatic plus zero-point-energy (ZPE) correction methods. Figure 2 illustrates the energy gaps among the eight spin configurations of the species. As shown in Fig. 2, the relative energies of the eight spin configurations are variable, depending on the spin coupling modes, although the optimized geometries are not so different (see SI). The energy gaps between the ground (↑↓↓↑) and excited (↑↓↑↓) spin configurations are only 0.18, 0.16 and 0.11 (kcal/mol), respectively, by the vertical, adiabatic, and adiabatic + ZPE methods. The triplet spin configuration (↑↓↓↑) (^{2}H)(S_{total} = (4-3-3+4)/2=2/2) is the ground state for the right (R)-opened structure $\mathbf{S_{1a}}$(R) with the mixed-valence (MV) configuration: Ca(II)Mn(III)$_a$Mn(IV)$_b$Mn(IV)$_c$Mn(III)$_d$. This trend is independent on the above computational procedures at the level of the broken-symmetry (BS) approximation. The singlet spin (S_{total} =(4-3+3-4)/2=0/2) configuration (↑↓↑↓) is the lowest excited configuration for $\mathbf{S_{1a}}$(R) with very small excitation energy (<0.2 kcal/mol).

Fig.2

The situation is reversed in the case of the proton-shifted structure $\mathbf{S_{1b}}$(C)(X=Y=OH) (Table S5) as illustrated in Fig. 3. The singlet (↑↓↑↓) spin configuration becomes the ground state under the adiabatic and adiabatic plus ZPE correction methods. However, the energy gaps between the ground singlet (↑↓↑↓) and excited triplet (↑↓↓↑) spin configurations are only 0.01, 0.02 and 0.05 (kcal/mol), respectively, by the vertical, adiabatic, and adiabatic + ZPE methods. Moreover the energy gaps between the low (↑↓↑↓) and intermediate (↑↑↑↓) spin configurations are -0.04, 0.09 and 0.14 (kcal/mol), respectively, by these methods. Thus three configurations are nearly degenerated in energy at the level of broken-symmetry UB3LYP, indicating the necessity of the exact diagonalization of the spin Hamiltonian matrix for elucidation of the reliable energy levels.

Fig.3

III.2 Theoretical calculations of effective exchange integrals

The energy gaps in Fig. 2 are mapped into spin Hamiltonian models (see supporting SIII).[45-52] Table 1 summarizes the calculated J values for $\mathbf{S_{1a}}$(R) (X=O;Y=H_2O). Using analytic computational formula (see eq. (S3), the exchange integrals were calculated to be -69.9, 2.77, 0.55, 20.4, 10.6 and -33.8 (cm^{-1}) for J_{ab}, J_{ac}, J_{ad}, J_{bc}, J_{bd} and J_{cd}, respectively, under the assumption of the vertical energy gap where the HS geometry was assumed for all other spin configurations. The corresponding

values obtained by the generalized approximate spin projection (GAP) method[53,54] were -69.9, 2.55, 0.38, 20.1, 7.79 and -33.5 (cm^{-1}), respectively. The sign and magnitude of the J_{pq} values obtained by these procedures are quite similar: the same situations are indeed concluded for adiabatic and adiabatic + ZPE gaps in Table 1. The quantum spin corrections for the J_{pq} values by the GAP procedure are small in the case of the $CaMn_4O_5$ cluster in OEC of PSII since the sizes of spins are 4/2 for Mn(III) and 3/2 for Mn(IV), respectively, indicating the classical spins.[49]

Table 1

Next we have examined the effect of full geometry optimizations. The J_{ab}, J_{ac}, J_{ad}, J_{bc}, J_{bd} and J_{cd} integrals for $\mathbf{S_{1a}}$(R)(X=O;Y=H_2O) are -77.1(-75.5), 2.91(3.06), 0.11(-0.33), 18.4(14.4), 6.84(4.95) and -35.6(-35.9) (cm^{-1}), respectively, by the GAP method based on the adiabatic energy gap, where the corresponding values by the adiabatic + ZPE gaps are given in parentheses. The J_{ab} and J_{cd} values are negative in sign in accord with the anti-ferromagnetic (anti-parallel) spin alignment (↑↓↓↑) of the ground state of the right (R)-opened structure, $\mathbf{S_{1a}}$(R). On the other hand, the J_{bc} value is positive in sign, in consistent with the ferromagnetic spin alignment between the b- and c-sites. Such qualitative tendencies are independent on the three different energy levels in Fig. 2. However the magnitude of the J value is different among them.

The energy gaps in Fig. 3 are mapped into spin Hamiltonian models (see supporting SIII). Table 2 summarizes the calculated J values for $\mathbf{S_{1b}}$(C)(X=Y=OH). The J_{ab}, J_{ac}, J_{ad}, J_{bc}, J_{bd} and J_{cd} values were calculated to be -8.50(-8.50), -0.29(0.51), -4.04(-3.88), 2.52(2.81), -2.33 (-2.11) and -37.4(-37.6) (cm^{-1}), respectively, by the analytical method under the assumption of the adiabatic + ZPE correction method, where the corresponding values by GAP are given in parentheses. The sign and magnitude of the J_{pq} values obtained by these procedures are quite similar. The analytical expression is useful for theoretical understanding of the origins of J values as formulated in eq. (S3).

Table 2

The J_{ab}, J_{ad} and J_{cd} values are negative in sign in accord with the anti-ferromagnetic (anti-parallel) spin alignment (↑↓↑↓) of the ground state of $\mathbf{S_{1b}}$(C). On the other hand, the J_{bc} value remains positive in sign, though its magnitude is largely reduced as compared with that of $\mathbf{S_{1a}}$(R) with the ferromagnetic spin alignment (↑↓↓↑) between the b- and c-sites. The magnitude of the negative J_{ab} integral (-8.5 cm^{-1}) for $\mathbf{S_{1b}}$(C) is also reduced significantly by protonation of the $O_{(5)}$ site of $\mathbf{S_{1a}}$(R), for which J_{ab} = -77.5 cm^{-1} in accord with general tendency for manganese complexes.[1-40] On the other hand, J_{cd} values are -37.6 and -35.9 (cm^{-1}) for $\mathbf{S_{1a}}$(R) and $\mathbf{S_{1b}}$(C), respectively, indicating no

change in accord with almost the same Mn_c-Mn_d distances of these structures. Thus the J values are sensitive to the geometries of the $CaMn_4O_4X(H_2O)_3Y$ cluster.

III.3 Energy levels by the exact diagonalizations

The energy gaps obtained by BS DFT in Fig. 2 provide a mean-field picture for relative stabilities among spin configurations. However, exact diagonalization of spin Hamiltonian model[72,73] consisted of the calculated J values are crucial for elucidation of quantum energy levels that are used for comparisons with excitation energies observed by spectroscopic methods such as EPR. The dimension of the spin Hamiltonian matrix becomes 400=5x4x4x5 where 5(=2(4/2)+1 for Mn(III) and 4(=2(3/2)+1) for Mn(IV) in the S_1 state. Table 3 summarizes the excitation energies and spin densities obtained for $\mathbf{S_{1a}}$(R)(X=O; Y= H_2O) by the exact diagonalization method. Figure 4 illustrates the energy levels of the ground and lower excited states for $\mathbf{S_{1a}}$(R). From Fig. 4, the ground state is triplet (S=1) under assumption of the vertical and adiabatic energy gaps. However the energy gaps between the ground triplet (S=1) and excited singlet (S=0) states are only 1.59 and 0.14 (cm^{-1}), respectively, by these approximations. The situation is reversed under the adiabatic + ZPE correction approximation, showing the singlet ground state with small triplet excitation energy; 2.88 cm^{-1}. The last result by adiabatic plus ZPE method is consistent with the parallel EPR results by Yamauchi et al[22] for the S_1 state: the signal at g=4.8 originates from an excited state with triplet spin state (S=1) with separation from the diamagnetic ground state (S=0) of about 1.74 cm^{-1}. Thus full geometry optimizations followed by the ZPE correction becomes crucial for quantitative discussions of the energy level in the S_1 state for OEC of PSII.

Table 3, Figure 4

Table S7 summarizes the excitation energies and spin densities obtained for $\mathbf{S_{1b}}$(C)(X=Y=OH) by the exact diagonalization method. Figure S1 illustrates the energy levels of the ground and lower-lying excited states for $\mathbf{S_{1b}}$(C). The ground state is singlet (S=0) irrespective of the J parameter sets employed as shown in Table S7 and Fig. S1. The energy gaps between the ground singlet and excited triplet states are 2.51, 14.0 and 15.5 (cm^{-1}), respectively, by the vertical, adiabatic and adiabatic + ZPE approximations. The excitation energy is larger than 15 cm^{-1} by the adiabatic + ZPE approximation. This means that the thermal excited triplet state cannot be detected at the low-temperature EPR experiment. As shown previously,[42] the $\mathbf{S_{1a}}$(R) (X=O; Y=H_2O) and $\mathbf{S_{1b}}$(C) (X=Y=OH) structures were nearly degenerated in energy in nonpolar condition. However the latter $\mathbf{S_{1b}}$(C) structure was calculated to be more stable than $\mathbf{S_{1a}}$(R) after the inclusion of polarization effect of methanol by the conductor PCM (CPCM) model.[42] Therefore significant increase of the weight of $\mathbf{S_{1b}}$(C) by

solvation effect of methanol is consistent with the disappearance of the parallel EPR signal for the methanol-treated S_1 state of OEC of PSII.[21,22]

III. 4 Theoretical calculations of spin densities

The calculated spin densities (Q) for the triplet state (S=1) of the right-opened structure, $\mathbf{S_{1a}}$(R)(X=O;Y=H_2O) obtained by twice of the projection factors in Table 3, are 1.74(1.98), -1.02(-1.02), -1.28(-1.22) and 2.30(2.26), respectively, by the vertical approximation, where the corresponding values by the adiabatic approximation are given in parentheses. The Q-values for the excited triplet state under the adiabatic + ZPE correction are 2.00, -1.02, -1.14 and 2.16, respectively,. The topology of the Q values for $\mathbf{S_{1a}}$(R) by the exact diagonalization is consistent with the spin alignment (↑↓↓↑) for the ground spin configuration in Fig. 2, supporting the BS approach to magneto-chemistry. This means that $\mathbf{S_{1a}}$(R) with the mixed-valence (MV) configuration $Mn(III)_aMn(IV)_b$ $Mn(IV)_cMn(III)_d$ in the S_1 state is an one-electron reduction state of the right-opened structure $\mathbf{S_{2a}}$(R) with the MV configuration $Mn(IV)_aMn(IV)_bMn(IV)_cMn(III)_d$ for the multiline g=2 spectra in the S_2 state. This is consistent with the conclusion of the EPR experiments[20-23] on the S_1 state.

IV Computational results for the S_3 state

IV.1 The optimized geometrical parameters of eight spin configurations

Tables S3 summarizes the optimized geometrical parameters for the water-inserted right-opened S_3 structure; $\mathbf{S_{3a}}$(R)-H_2O(X=O;Y=H_2O;W=OH) (see Fig. 1). From Table S3, the optimized Mn-Mn distances for $\mathbf{S_{3a}}$(R)-H_2O are almost the same for the eight spin configurations. The rule 'Ib' is also applicable for the optimized Mn-Mn distances of $\mathbf{S_{3a}}$(R)-H_2O. Table S4 summarizes the optimized geometrical parameters of the left (L)-opened water-inserted structure, $\mathbf{S_{3a}}$(L)-H_2O (X=O; Y= H_2O; W=OH). The optimized Mn-Mn distances for the eight-different spin configurations support the rule 'Ic' for the left-opened structure: $R(Mn_b\text{-}Mn_c) \sim R(Mn_c\text{-}Mn_d) < R(Mn_b\text{-}Mn_d) < R(Mn_a\text{-}Mn_b) < R(Mn_a\text{-}Mn_d)$. The $Mn(IV)_bMn(IV)_cMn(IV)_d$ triangle in the cubane fragment of $\mathbf{S_{3a}}$(L) is almost equilateral because of the absence of Jahn-Teller (JT) distortion of the Mn(III) ion[42], whereas it is obtuse in the $\mathbf{S_{1a}}$(R)(X=O;Y= H_2O) and $\mathbf{S_{1b}}$(C) (X=Y=OH), and high-resolution XRD structures[44] because of the JT distortion of $Mn(III)_d$. The Mn_b-Mn_d distance becomes shorter than that of the Mn_a-Mn_b distance in the L-opened structure. Details of the optimized geometrical parameters are given in supporting material (SI).

IV.2 Relative stabilities of the eight spin configurations

We consider magneto-structural correlations in the S_3 state of the Kok cycle. Table S6 summarizes the relative energies among the eight spin configurations for the

right-opened water-inserted structure $\mathbf{S_{3a}}$(R)-H_2O (X=O;Y=H_2O; W=OH) in the S_3 state on the basis of the vertical, adiabatic and adiabatic plus zero-point-energy (ZPE) correction methods. Figure 5 illustrates the energy gaps among the eight spin configurations of the species. As shown in Fig. 5, the relative energies of the eight spin configurations are variable, depending on the spin coupling modes although the optimized geometries are not so different (see section SIII). The singlet spin configuration (↑↓↓↑)(^{1}H) (S_{total} = (3-3-3+3)/2=0/2) remains the ground state irrespective of the computational methods. The energy gaps between the ground (↑↓↓↑) and excited intermediate (↓↑↑↑) (^{7}E) (S_{total} = (-3+3+3+3)/2=6/2) spin configurations are only 0.15, 0.26 and 0.32 (kcal/mol), respectively, by the vertical, adiabatic, and adiabatic + ZPE methods.

Fig. 5

The situation is reversed in the case of the left-opened water-inserted structure $\mathbf{S_{3a}}$(L)-H_2O (X=O; Y=H_2O; W=OH) (Table S6) as illustrated in Fig. 6. The septet spin configuration (S=3) (↓↑↑↑) (^{7}E) becomes the ground state irrespective of the computational procedures. The energy gaps between the ground septet (↓↑↑↑) and excited singlet (↑↓↓↑) spin configurations are 0.91, 0.78 and 0.58 (kcal/mol), respectively, by the vertical, adiabatic, and adiabatic + ZPE methods. Moreover the energy gaps between the ground septet (↓↑↑↑) and high-spin (HS) (↑↑↑↑) configurations are 0.38, 0.74 and 0.61 (kcal/mol), respectively, by these methods.

Fig. 6

IV.3 Theoretical calculations of effective exchange integrals

The energy gaps in Fig. 5 are mapped into spin Hamiltonian models (see supporting SIII).[53,54,72,73] Table 4 summarizes the calculated J values $\mathbf{S_{3a}}$(R)-H_2O (X=O;Y=H_2O; W=OH). The exchange integrals obtained are -17.3(-17.1), 0.39(0.29), 4.08(3.98), 8.93(8.82), -2.52(-2.62) and 0.78(0.87) (cm^{-1}) for J_{ab}, J_{ac}, J_{ad}, J_{bc}, J_{bd} and J_{cd}, respectively, by the analytical (see eq. (S9)) method under the assumption of the vertical energy gap, where the corresponding values by the generalized approximate spin projection (GAP) method are given in parentheses. The sign and magnitude of the J_{pq} values obtained by these procedures are quite similar: the same situations are also concluded for adiabatic and adiabatic plus ZPE energy gaps in Table S6.[45-52] The J_{ab}, J_{ac}, J_{ad}, J_{bc}, J_{bd} and J_{cd} integrals for $\mathbf{S_{3a}}$(R)-H_2O are -23.7(-25.4), 0.10(0.39), 3.98(4.08), 6.49(5.23), -3.20(-3.88) and -3.00(-4.46) (cm^{-1}), respectively, by the GAP method based on the adiabatic energy gaps, where the corresponding values by the adiabatic plus ZPE gaps are given in parentheses.

Table 4

The positive (ferromagnetic) J_{cd} value by the vertical gap is converted into the negative (antiferromagnetic) value after the full geometry optimizations, namely adiabatic approximation. Thus subtle geometry changes are not negligible for computations of J values. The negative J_{ab}, J_{bd} and J_{cd} values are in accord with the anti-ferromagnetic (anti-parallel) spin alignment (↑↓↓↑) of the ground state of $\mathbf{S_{3a}}$(R)-H_2O. On the other hand, the J_{bc} value is positive in sign, in consistent with the ferromagnetic spin alignment between the b- and c-sites.

The energy gaps in Fig. 6 are mapped into spin Hamiltonian models (see supporting SVII).[53,54,72,73] Table 5 summarizes the calculated J values $\mathbf{S_{3b}}$(L)-H_2O (X=O;Y=H_2O;W=OH). From Table 5, the analytical and GAP methods provide similar J values irrespective of the computational procedures of the energy gaps between the eight spin configurations. The J_{ab}, J_{ac}, J_{ad}, J_{bc}, J_{bd} and J_{cd} values were calculated to be -31.1(-30.7), 1.94(1.75), 5.44(5.25), 36.9(36.7), -8.93 (-9.12) and 36.9(37.1) (cm^{-1}), respectively, by the analytical eq. (S9) under the assumption of the adiabatic plus ZPE correction method, where the corresponding values by GAP are given in parentheses. The J_{ab} value is negative in sign in accord with the anti-ferromagnetic (anti-parallel) spin alignment (↓↑↑↑) of the ground state of $\mathbf{S_{3a}}$(L)-H_2O. On the other hand, the J_{bc} and J_{cd} values are largely positive in sign, with the ferromagnetic spin alignment in the b-c-d-line. Interestingly, the J_{bd} integral is negative in sign (-9 cm^{-1}).

Previously[73] we have examined the so-called (1+3) model[36] consisted of the outer Mn ion (A-part) and cubane fragment (B-part). The septet and HS configurations are regarded as the anti-(↓–↑↑↑) and ferro-(↑–↑↑↑) magnetic exchange coupled systems between the local HS $Mn(IV)_a$ monomer (A-part; S_A=3/2) and HS $Mn(IV)_b$ $Mn(IV)_cMn(III)_d$ trimer (B-part; S_B=9/2) in this model.[36,73] The exchange coupling constants (J_{AB}) for the model are calculated to be -4.43, -8.62 and -7.10 (cm^{-1}), respectively, by using the energy gaps obtained for these configurations. The J values become negative in sign in conformity with the ferrimagnetic (↓–↑↑↑) ground state, affording the total intermediate spin configuration (S_{total}=9/2-3/2=3).

Christou et al[74] have synthesized the cubane-like model complex, $Ca_2Mn(IV)_3O_4$ and have observed the magnetic susceptibility in the 5.0-300 K range, elucidating the ferromagnetic (↑↑↑) gound state (S=9/2). The curve fitting of the susceptibility has revealed that the observed J_{bc}, J_{bd} and J_{cd} integrals are 40.5(36.7), -10.8(-9.12) and 40.5(371.) (cm^{-1}), respectively, where the corresponding calculated J values for $\mathbf{S_{3a}}$(L)-H_2O are given in parentheses. The observed and calculated J values are similar, indicating that $\mathbf{S_{3a}}$(L)-H_2O has a similar cubane skeleton to that of the model complex by Christou et al.[74]

Table 5

IV.3 Energy levels by the exact diagonalizations

The energy gaps in Figs. 5 and 6 provide a mean-field picture for relative stabilities among spin configurations. The exact diagonalization of spin Hamiltonian model has been performed for quantitative purpose. The dimension of the spin Hamiltonian matrix becomes 256=4x4x4x4 where 4(=2(3/2)+1) for Mn(IV) in the S_3 state. Table 6 summarizes the excitation energies and projection factors obtained for $\mathbf{S_{3a}}$(R)-H_2O (X=O;Y=H_2O; W=OH) by the method. Figure S2 illustrates the energy levels of the ground and lower excited states for $\mathbf{S_{3a}}$(R)-H_2O. The ground state is singlet (S=0) irrespective to the computational procedures as shown in Fig. S2. However the energy gaps between the ground singlet and excited triplet (S=1) states are only 2.47, 8.06 and 10.1 (cm^{-1}), respectively, by the vertical, adiabatic and adiabatic plus ZPE correction methods.

Table 6

Matsukawa et al[24] have observed the parallel polarization EPR signals at g=12 and 8 for the S_3 state of OEC of PSII. Temperature dependence of the signal intensity has revealed that the signals arise from a low-lying triplet (S=1) excited state. Present computational results for $\mathbf{S_{3a}}$(R)-H_2O suggest that the thermally excited triplet (S=1) observed by Matsukawa et al[24] may be assigned as that of a right-opened structure in the S_3 state of OEC of PSII. The relatively large gap is also compatible with rapid disappearance of the ESR spectra in the case of the methanol-treated experiments. Thus the $\mathbf{S_{3a}}$(R)-H_2O structure is regarded as one-electron oxidation state of the $\mathbf{S_{2a}}$(R) structure with the doublet ground state characterized with the multiline g=2 spectra.[1-40]

Table 7 summarizes the excitation energies and projection factors obtained for the left-opened water-inserted structure $\mathbf{S_{3a}}$(L)-H_2O (X=O;Y=H_2O; W=OH) by the exact diagonalization method. Figure 7 illustrates the energy levels of the ground and lower-lying excited states for $\mathbf{S_{3a}}$(L)-H_2O. From Fig. 7, the ground state is septet (S=3) irrespective of the J parameter sets employed. The energy gaps between the ground septet (S=3) and excited nanet (S=4) states are 26.8, 50.1 and 39.1 (cm^{-1}), respectively, by the vertical, adiabatic and adiabatic plus ZPE approximations. The excitation energy is larger than 25 cm^{-1}. This means that the thermally excited higher-spin state (S=4) cannot be detected at the low-temperature EPR experiment. The $\mathbf{S_{3a}}$(L)-H_2O structure is regarded as one-electron oxidation state of the $\mathbf{S_{2a}}$(L) structure with the sextet (S=5/2) ground state characterized by the g=4.1 spectra.[1-40]

Boussac et al[26] have revealed the complete EPR spectrum involving g=8 and g=4 signals in the S_3 state. Simulations of the spectrum have indicated that the S_3

experimental EPR spectrum is associated with a pure sextuplet (S=3) spin system and not with a triplet (S=1) state.[24] Present computational results suggest that the sextuplet EPR spectra observed by Boussac et al[26] is responsible for the left-opened structure in the S_3 state. Unfortunately Boussac et al[26] has not elucidated the temperature dependence of the intensity of the sextuplet EPR signal, although our computational results predict that the signal arises from the ground sextuplet (S=3) state.

Table 7, Figure 7

IV. 4 Theoretical calculations of spin densities

The calculated spin densities (Q) provide information on the topology of spin alignments in the $CaMn_4O_5$ cluster of OEC of PSII; the Q values for the triplet state are twice of the projection factors in Table 7. The calculated Q values for the first-excited triplet state (S=1) of the right-opened water-inserted structure, $\mathbf{S_{3a}}$(R)-H_2O (X=O;Y=H_2O; W=OH), are 0.12(0.24), 0.12(0.04), 0.88(0.88) and 0.88(0.84), respectively, by the vertical approximation, where the corresponding values by the adiabatic approximation are given in parentheses. The spin densities on the $Mn(IV)_a$ and $Mn(IV)_b$ ions are almost zero, indicating the localization of spin density on the $Mn(IV)_a$ and $Mn(IV)_b$ ions. The topology of the Q populations is different from the spin alignment (↑↓↓↑) for the ground low-spin (LS) broken-symmetry (BS) configuration of $\mathbf{S_{3a}}$(R)-H_2O.

The spin densities (Q=6 x spin projection factor) for the ground septet (S=3) state of the left-opened water-inserted structure, $\mathbf{S_{3a}}$(L)-H_2O (X=O;Y=H_2O; W=OH), are -1.68(-1.50), 1.92(1.68), 2.82(2.76) and 3.00(3.00), respectively, as shown in Table 7 by the adiabatic approximation, where the corresponding values by the adiabatic + ZPE approximation are given in parentheses. The topology of the spin densities for $\mathbf{S_{3a}}$(L)-H_2O is consistent with the spin alignment (↓↑↑↑) of the ground broken-symmetry (BS) solution in Fig. 6, indicating that the ground BS solution is reasonable as a first step for theoretical understanding of the spin states of $\mathbf{S_{3a}}$(L)-H_2O.

V Discussions and concluding remarks

V. 1 Comparison with the EXAFS structure

Since the report of the PSII XRD structure at the 1.9 Å resolution,[44] the structural studies on OEC of PSII have dramatically advanced. However, at present, the reported OEC structures by XRD are only in the static S_1 state[44,75-83], where EPR experiments[1-40] have been reported as discussed in the previous sections. On the other hand, EXAFS results have provided essential structural information for the S_1 and S_3 state. The EXAFS results for the S_1 state[84-89] showed that the Mn_a-Mn_b, Mn_b-Mn_c, Mn_c-Mn_d, Mn_b-Mn_d and Mn_a-Mn_d distances are 2.71(2.69), 2.79(2.77), 2.71(2.73), 3.28(3.27) and

4.79(4.78) (Å), respectively, where the corresponding values (average of the eight spin configurations in Table S1) calculated for $\mathbf{S_{1a}}$(R)(X=O;Y=H_2O) are given in parentheses. The calculated Mn-Mn distances are well consistent with the EXAFS values. On the other hand, the Ca-Mn_a, Ca-Mn_b, Ca-Mn_c and Ca-Mn_d distances by EXAFS[89] (calculated values are given in parentheses) are 3.99(3.63), 3.36(3.40), 3.36(3.29) and 3.36(3.52) (Å), respectively. The Ca-Mn_a distance by EXAFS is a little longer than the calculated (3.63) and XRD (3.79)[44] values.

The average Mn_a-Mn_b, Mn_b-Mn_c, Mn_c-Mn_d, Mn_b-Mn_d and Mn_a-Mn_d distances calculated for the proton-shifted structure $\mathbf{S_{1b}}$(R)(X=Y=OH) are 2.94(2.97), 2.79(2.89), 2.71(2.84), 3.43(3.29) and 5.37(5.00) (Å), respectively, where the corresponding values by the high-resolution XRD are given in parentheses. The calculated Mn_b-Mn_c and Mn_c-Mn_d distances are shorter by about 0.1 Å than the XRD values[44], although they are consistent with the corresponding EXAFS values. This entails two different opinions on the XRD structure:[44] one is that such small difference is within the error bar (0.16 Å) at the 1.9 Å resolution of the XRD experiment. The other is that the difference may be caused by the X-ray damage of the XRD structure.[56-67,89] We have thoroughly examined several possible explanations on the basis of accumulated XRD, EXAFS and computational results.[42,43,50-52] The key point is that the protonation of the $O_{(5)}$ is necessary for reproduction of the XRD structure[44] although protonation of other oxygen dianions ($O_{(1)}$, $O_{(2)}$, $O_{(3)}$ and $O_{(4)}$) are not necessary in contradiction to the claim by Knapp et al[63] that the XRD structure is not in the S_1 state, but in the S_{-3} state. Therefore more refined XRD structures are really desirable for deeper understanding of the X-ray damages.[84-89]

The average Mn_a-Mn_b, Mn_b-Mn_c, Mn_c-Mn_d, Mn_b-Mn_d and Mn_a-Mn_d distances calculated for the right-opened water-inserted structure $\mathbf{S_{3a}}$(R)-H_2O(X=O;Y=H_2O,W=OH) are 2.70(2.75), 2.78(2.79), 2.79(2.75), 3.38(3.26) and 5.31 (Å), respectively, where the corresponding values by the recent model A based on the EXAFS[89] are given in parentheses. The $Mn_bMn_cMn_d$ triangle is obtuse for $\mathbf{S_{3a}}$(R)-H_2O and the model A is in consistent with the R-opened structure. The Ca-Mn_a, Ca-Mn_b, Ca-Mn_c and Ca-Mn_d distances for $\mathbf{S_{3a}}$(R)-H_2O (model A) are 3.98(3.99), 3.58(3.37), 3.39(3.37) and 3.38(3.37) (Å), respectively. The Ca-Mn_a distance for the model A[89] is consistent with the calculated value because recently refined EXAFS results provide a new structure similar to XRD[44].

The average Mn_a-Mn_b, Mn_b-Mn_c, Mn_c-Mn_d, Mn_b-Mn_d and Mn_a-Mn_d distances calculated for the left-opened water-inserted structure $\mathbf{S_{3a}}$(L)-H_2O (X=O; Y=H_2O, W=OH) are 3.22(2.82), 2.73(2.72), 2.72(2.72), 2.84(2.82) and 5.24 (Å), respectively,

where the corresponding values by the recent model B based on the EXAFS[89] are given in parentheses. The $Mn_bMn_cMn_d$ triangle is almost equilateral for $\mathbf{S_{3a}}$(L)-H_2O and the model B in consistent with the L-opened structure. Recently Christou et al.[74] have synthesized the model complex, $Ca_2Mn(IV)_3O_4$, for which the Mn_b-Mn_c, Mn_c-Mn_d, and Mn_b-Mn_d distances by XRD are 2.76, 2.73 and 2.86 Å, respectively. The experimental Mn-Mn distances are consistent with those of $\mathbf{S_{3a}}$(L)-H_2O and the model B.[89] The Ca-Mn_a, Ca-Mn_b, Ca-Mn_c and Ca-Mn_d distances for $\mathbf{S_{3a}}$(L)-H_2O (model B) are 4.39(3.99), 3.42(3.34), 3.46(3.34) and 3.42(3.34) (Å), respectively. The calculated Ca-Mn_a distance for $\mathbf{S_{3a}}$(L)-H_2O is longer than that of the model B based on EXAFS.[89]

V.2 Generation of radical species in the S_3 state

XPS experiments by Berkeley group[84-89] have shown that the oxidation of the Mn site in the $CaMn_4O_5$ cluster of OEC of PSII is hardly conceivable in the S_2-S_3 transition because of very small shift of the X-ray absorption spectra, indicating a hole generation in a core oxygen site or a ligand site. The reduction of one of Mn(IV) ions is an interesting problem in relation to the internal reduction[59] of Mn ion instead of its external reduction by the X-ray radiation. However the water-inserted structures $\mathbf{S_{3a}}$(R)-H_2O and $\mathbf{S_{3a}}$(L)-H_2O examined in this paper are responsible for the oxidation of Mn(III) site in the S_2 structures $\mathbf{S_{2a}}$(R) and $\mathbf{S_{2a}}$(L), indicating the uniform valence structure $Mn(IV)_aMn(IV)_b Mn(IV)_cMn(IV)_d$.

Previous BS DFT computations[42] have revealed that the one-electron transfer from hydroxide anion to the $CaMn(IV)_4O_5$ core is feasible in the S_3 state, affording the radical-coupled structures as illustrated in Fig. 8. For example, the hydroxyl anion coordinated to the $Mn(IV)_a$ ion without hydrogen-bonding stabilization affords one electron to the $Mn(IV)_d$ ion in the right-opened structure, providing a $\mathbf{S_{2a}}$(R)-OH•(Mn_a) species with the mixed-valence configuration $Mn(IV)_aMn(IV)_bMn(IV)_c Mn(III)_d$ in Fig. 8A. Similarly the hydroxyl anion coordinated to the Ca(II) ion affords one electron to the $Mn(IV)_d$ ion in the right-opened structure, providing a $\mathbf{S_{2a}}$(R)-OH•(Ca) in Fig. 8B. The ground spin configuration of these species is predicted to be singlet as illustrated in the spin alignments that consist of doublet radical with down-spin (•↓) and total doublet right (R)-opened structure $\mathbf{S_{2a}}$(R)(X=O: Y= H_2O) in the S_2 state. Therefore these singlet structures are possible candidates for the diamagnetic ground state species proposed by Matsukawa et al[21] and Ioannidia et al.[22]

The proton shift from hydroxyl anion (W=OH) to the other hydroxyl anion (Y=OH) to afford Mn(IV)-oxo bond and Y=H_2O might be possible in the water-inserted structures $\mathbf{S_{3a}}$(R)-H_2O and $\mathbf{S_{3a}}$(L)-H_2O, in Fig. 1 when water molecule at the Y-site is deprotonated in the S_2 state as postulated in several papers.[37,38] The high-valent

Mn-oxo species often exhibit the oxyl radical character as illustrated in Fig. 8C and 8D. The left-opened structure $\mathbf{S_{2a}}$(L)-O•(Mn_a) in Fig. 8C is regarded as an exchange-coupled state consisted of the oxyl-radical with the up-spin (•↑) and total sextet (S=5/2) left-opened structure $\mathbf{S_{2a}}$(L)[41,42] with the mixed valence configuration $Mn(III)_aMn(IV)_b$ $Mn(IV)_cMn(IV)_d$. The ground spin configuration of the coupled structure $\mathbf{S_{2a}}$(L)-O•(Mn_a) is septet (S=3) as illustrated in Fig. 8C, indicating a possible candidate for the high-spin species observed by Boussac et al.[26] On the other hand, the right-opened structure $\mathbf{S_{2a}}$(R)-O•(Mn_d) in Fig. 8D is regarded as an exchange-coupled state consisted of the oxyl-radical with the down-spin (•↓) and total doublet (S=1/2) right-opened structure $\mathbf{S_{2a}}$(R)[41,42] with the mixed valence configuration $Mn(IV)_aMn(IV)_b$ $Mn(IV)_cMn(III)_d$. Therefore this structure is totally singlet, indicating a possible candidate for the diamagnetic species proposed by Matsukawa et al[24] and Ioannidia et al.[25] The present computational results provide guiding principles for further experimental studies of the ground S=0 or S=3 species in the S_3 state in future.

V. 3 Right- and left-handed scenario for water oxidation

Present BS DFT computations have revealed the magneto-structural correlation in the S_3 state that is the final step observed by the EPR spectroscopy. The right (R)- and left (L)-opened structures revealed[41-43] open right- and left-handed scenarios for the O-O bond formations of water oxidation in OEC of PSII. Past several years, Siegbahn[56-59] has theoretically investigated the R-handed scenario for the water splitting reaction, proposing several transition structures for water oxidations. However, the present computational results have shown that the L-handed scenario presented by several groups[33,45-52,73, 90-92] in past decades still remains as a possible route for water oxidation. For example, the O-O bond formation is conceivable via the radical addition of oxyl-radical O• to $O_{(5)}$ site in both L- and R-scenario as can be seen in Fig. 8C and 8D.

The one-electron oxidation of the Mn(III) site in the S_3 to S_4 transition affords a reactive Mn(IV)-O• bond (see Fig. S3) as illustrated in Fig. 8E and 8F. The radical coupling (RC) mechanism is conceivable in this situation, where the local singlet diradical (LSD) configuration (O•↑...↓•O) can be formed in the transition-state (TS) region. We have already examined a number of the radical coupling (RC) modes (see for example, Fig. 6 in ref. 92 and Fig. 10 in ref. 52) even in the Berkeley[84], Berlin[75] and other structural models[44,76-82] to elucidate spin correlation diagrams for the O-O bond formation and release of triplet molecular oxygen. The magnetic coupling modes were found to be closely related to formation of singlet or triplet molecular oxygen.[92] Thus magneto-structural correlations are also important in the transition state region for the O-O bond formation.

V. 4 Concluding remark

The energy levels for the right-opened structure S_{1a}(R)(X=O; Y=H_2O) in Fig. 1A have been elucidated by the exact diagonalization of the spin Hamiltonian matrix consisted of the effective exchange integrals (J) determined by the generalized approximated spin projection (GAP) procedure based on energy levels by adiabatic plus zero point energy (ZPE) correction UB3LYP method. The calculated excitation energy (2.88 cm^{-1}) between the ground singlet and excited triple states is consistent with the corresponding energy gap (1.74 cm^{-1}) revealed by the EPR experiment in the S_1 state.[21,22] On the other hand, the energy levels for the left-opened water-inserted structure S_{3a}(L)-H_2O(X=O; Y=H_2O; W=OH) in Fig. 1D obtained by the same GAP procedure have indicated the septet (S=3) ground state, for which the excitation energy between the ground (S=3) and excited (S=4) spin state is larger than 25 cm^{-1}. The computational results for S_{3a}(L)-H_2O is compatible with the septet (S=3) spin state observed by the EPR spectroscopy.[26] Thus present BS DFT followed by the exact diagonalization[72,73] is useful for elucidation of the magneto-structural correlations in the S_1 and S_3 states of OEC of PSII.

The energy gap between the ground singlet and excited triplet states is calculated to be larger than 15 cm^{-1} for proton-shifted structure S_{1b}(C)(X=Y=OH) in Fig. 1B in the S_1 state, suggesting the ESR silent state in the low-temperature region. This is not incompatible with the observation of disappearance of the EPR spectra after the methanol treatment of OEC of PSII in the S_1 state.[22] Previous CPCM/UB3LYP computations[42] including polarization effect of methanol have indeed revealed that the S_{1b}(C)(X=Y=OH) structure becomes more stable than the S_{1a}(R)(X=O;Y=H_2O) structure in such polarized state. Similarly the energy gap between the ground singlet and excited triplet states is larger than 25 cm^{-1}, namely ESR-silent, for the right-opened water-inserted structure S_{3a}(R)-H_2O(X=O; Y=H_2O; W=OH) in Fig. 1C in the S_3 state. This may support the observation that the methanol treatment of OEC of PSII in the S_3 state entails the disappearance of the EPR spectra[24,25] under the assumption of the greater stability of S_{3a}(R)-H_2O than S_{3a}(L)-H_2O in the polar condition. Present computational results provide guiding principles for further refined EPR experiments of OEC of PSII in the S_1 and S_3 states under several different environmental conditions.

Acknowledgements

This work has been supported by a Grants-in-Aid for Scientific Research (C). No. 2355016 (to SY) and a Grants-in-Aid for Specially Promoted Research No. 24000018 (to MS, JRS and KY) by the Ministry of Education, Culture, Sports, Science and

Technology (MEXT) of Japan.

References

1. G. C. Dismukes, Y. Siderer, Proc. Natl. Acad. Sci. USA, 1891, **78**, 274-278.
2. O. Hansson and L. –E. Andreasson, Biochim. Biophy. Acta, 1982, **679**, 261-268.
3. J. L. Casey, K. Sauer, Biochim. Biophys. Acta 1984, **767**, 21-28.
4. J. L. Zimmerman, A. W. Rutherford, Biochim. Biophys. Acta 1984, **767**, 160-167.
5. J. C. de Paula, W. F. Beck, G. W. Brudvig, J. Am. Chem. Soc. 1986, **108**, 4018-4022.
6. D. H. Kim, R. D. Britt, M. P. Klein, K. Sauer, J. Am. Chem. Soc. 1990, **112**, 9389-9391.
7. D. H. Kim, R. D. Britt, M. P. Klein, K. Sauer, Biochemistry, 1992, **31**, 541-547.
8. A. Haddy, W. R. Dunham, R. H. Sands, R. Aasa, Biochim. Biophys. Acta 1992, **1099**, 25-34.
9. K. A. Ahrling, P. J. Smith, R. J. Pace, J. Am. Chem. Soc. 1986, **120**, 13202-13213.
10. K. A. Ahrling, R. J. Pace, Biophys. J. 1995, **68**, 2181-2189.
11. J. Messinger, J. H. A. Nugevt, M. C. W. Evans, Biochemistry, 1997, **36**, 11055-11060.
12. K. A. Åhrling, S. Peterson, S. Styring, Biochemistry, 1997, **36**, 13148-13152.
13. D. A. Force, D. W. Randall, G. A. Lorigan, K. L. Clemens, R. D. Britt, J. Am. Chem. Soc. 1998, **120**, 13321-13333.
14. A. Boussac, J. –J. Girerd, A. W. Rutherford, Biochemistry, 1996, **35**, 6984-6989.
15. A. Boussac, S. Un, O. Horner, A. W. Rutherford, Biochemistry, 1998, **37**, 4001-4007.
16. A. Boussac, H. Kuhl, E. Ghibaudi, M. Rogner, A. W. Rutherford, Biochemistry, 1999, **38**, 11942-11948.
17. K. Hasegawa, M. Kusunoki, Y. Inoue, T. –A. Ono, Biochemistry, 1998, **37**, 9457-9465.
18. K, Hasegawa, T. –A. Ono, Y. Inoue, M. Kusunoki, Chem. Phys. Lett. 1999, **300**, 9-19.
19. M. F. Charlot, A. Boussac, G. Blondfin, Biochim. Biophy. Acta, 2005, **1708**, 120-132.
20. S. L. Dexheimer and M. P. Klein, J. Am. Chem. Soc. 1992, **114**, 2821-2826.
21. D. Koulougiotis, D. J. Hitsh and G. W. Brudvig, J. Am. Chem. Soc. 1992, **114**, 8322-8323.

22. T. Yamauchi, H. Mino, T. Matsukawa, A. Kawamori and T. Ono, Biochemistry, 1997, 36-7520-7526.
23. K. A. Campbell, J. M. Peloquin, D. P. Pham, R. J. Debus and R. D. Britt, J. Am. Chem. Soc. 1992, **114**, 8322-8323.
24. T. Matsukawa, H. Mino, D. Yoneda, A. Kawamori, Biochemistry, 1999, **38**, 4072-4077.
25. N. Ionnnidis and V. Petrouleas, Biochemistry, 2000, **39**, 5246-5254.
26. A. Boussac, M. Sugiura, W. Rutherford and P. Dorlet, J. Am Chem. Soc. 2009, **131**, 5050-5051.
27. M. Zheng, G. C. Dismukes, Inorg. Chem. 1996, **35**, 3307-3319.
28. J. M. Peloquin, K. A. Campbell, D. W. Randall, M. A. Evanchik, R. D. Britt, J. Am. Chem. Soc. 2000, **122**, 10926-10942.
29. J. M. Peloquin, R. D. Britt, Biochim. Biophys. Acta 2001, **1503**, 96-111.
30. R. D. Britt, J. M. Peloquin, K. A. Campbel, Annu. Rev. Biophy. Biomol. Struct. 2000, **29**, 463–95.
31. J. M. Peloguin, K. A. Campbell, D. W. Randall, M. A. Evanchik, V. L. Pecoraro, W. H. Armstrong, R. D. Britt, J. Am. Chem. Soc. 2000, **122** 10926-10942
32. C. P. Aznar, R. D. Britt, Phil. Trans. R. Soc. Lond., 2002, **B357**,1359-1366.
33. R. D. Britt, K. A. Cambell, J. M. Peloguin, M. L. Gilchrist, C. P. Aznar, M. M. Dicus, J. Robblee, J. Messinger, Biochem. Biophys. Acta, 2004, **1655** 158-171.
34. L. V. Kulik, B. Epel, W. Lubitz, J. Messinger, J. Am. Chem. Soc. 2005, **127**, 2392-2393.
35. L. V. Kulik, B. Epel, J. Messinger, Biochemistry, 2005, **44**, 9368-9374.
36. L. V. Kulik, B. Epel, W. Rubitz, J. Messinger, J. Am. Chem. Soc. 2007, **129** 13421-13435.
37. N. Cox, L. Rapatskiy, J.-H. Su, D. A. Pantazis, M. Sugiura, L. Kulik, P. Dorlet, A. W. Rutherford, F. Neese, A. Boussac, W. Lubitz, J. Messinger, J. Am. Chem. Soc. 2011, **133**, 3635-3648.
38. W. Ames, D. A. Pantazis, V. Krewald, N. Cox, J. Messinger, W. Lubitz, F. Neese, J. Am. Chem. Soc. 2011, **133**, 19743-19757.
39. T. A. Stich, G. J. Yeagle, R. J. Service, R. J. Debus, R. D. Britt, Biochemistry 2012, **50**, 7390-7404.
40. L. Rapatskiy, N. Cox, A. Savitsky, W. A. Ames, J. Sander, M. N. Nowaczyk, M. Rogner, A. Boussac, F. Neese, J. Messinger, W. Lubitz, J. Am. Chem. Soc.

2012, **134**, 16619-16634.
41. D. A. Pantazis, W. Ames, N. Cox, W. Lubits, F. Neese, Angew. Chem. Int. Ed. 2012, **51**, 9935-9941.
42. H. Isobe, M. Shoji, S. Yamanaka, Y. Umena, K. Kawakami, N. Kamiya, J. –R. Shen, K. Yamaguchi, Dalton Trans. 2012, **41**, 13727-13740.
43. M. Shoji, H. Isobe, S. Yamanaka, Y. Umena, K. Kawakami, N. Kamiya, J.-R. Shen, K. Yamaguchi, Catl. Sci. Technol. 2013, **3**, 1831-1848.
44. Y. Umena, K. Kawakami, J. –R. Shen, N. Kamiya, Nature 2011, **473**, 55-60.
45. K. Kanda, S. Yamanaka, T. Saito, Y. Umena, K. Kawakami, J. R. Shen, N. Kamiya, M. Okumura, H. Nakamura, K. Yamaguchi, Chem. Phys. Lett. 2011, **506**, 98-103.
46. S. Yamanaka, H. Isobe, K. Kanda, T. Saito, Y. Umena, K. Kawakami, J. R. Shen, N. Kamiya, M. Okumura, H. Nakamura, K. Yamaguchi, K. Chem Phys Lett 2011, **511**, 138-145.
47. T. Saito, S. Yamanaka, K. Kanda, H. Isobe, Y. Takano, Y. Shigeta, Y. Umena, K. Kawakami, J. R. Shen, N. Kamiya, M. Okumura, M. Shoji, Y. Yoshioka, K. Yamaguchi, Int. J. Quant. Chem. 2012, **112**, 253-276.
48. S. Yamanaka, T. Saito, K. Kanda, H. Isobe, Y. Umena, K. Kawakami, J. R. Shen, N. Kamiya, M. Okumura, H. Nakamura, K. Yamaguchi, Int. J. Quant. Chem. 2012, **112**, 321-343.
49. S. Yamanaka, K. Kanda, T. Saito, Y. Umena, K. Kawakami, J. –R. Shen, N. Kamiya, M. Okumura, H. Nakamura, K. Yamaguchi, Adv. Quant. Chem. 2012, Vol **64**, 121-187.
50. K. Yamaguchi, S. Yamanaka, T. Saito, K. Kanda, H. Isobe, M. Shoji, Y, Umeya, K. Kawakami, J. R. Shen, N. Kamiya, M. Okumura, Int. J. Qunat, Chem, 2013, **113**, 525-541.
51. K. Yamaguchi, S. Yamanaka, H. Isobe, T. Saito, K. Kanda, Y, Umeya, K. Kawakami, J. R. Shen, N. Kamiya, M. Okumura, H. Nakamura, M. Shoji, Y. Yoshioka, Int. J. Qunat, Chem, 2013, **113**, 453-473.
52. K. Yamaguchi, S. Yamanaka, M. Shoji, H. Isobe, Y. Kitagawa, T. Kawakami, S. Yamada, M. Okumura, Mol. Phys. 2013, Doi. Org. /10.1080/00268976. 2013.842009.
53. M. Shoji, K. Koizumi, T. Hamamoto, Y. Kitagawa, S. Yamanaka, M. Okumura, K. Yamaguchi, Chem. Phys. Lett. 2006, **421**, 483-487.
54. M. Shoji, K. Koizumi, Y. Kitagawa, S.Yamanaka, M. Okumura, K. Yamaguchi, Y. Ohki, Y. Sunada, M. Honda, K. Tatsumi, Int. J. Quant. Chem. 2006, **106**,

3288-3302.
55. T. Soda, Y. Kitagawa, T. Onishi, Y. Takano, Y. Shigeta, H. Nagao, Y. Yoshioka, K. Yamaguchi, Chem. Phys. Lett. 2000, **319**, 223-230.
56. P. E. M. Siegbahn, Acc. Chem. Res. 2009, **42**, 1871-1880.
57. P. E. M. Siegbahn, Photochem. J. Photobiol. 2011, **511**, 138-150.
58. P. E. M. Siegbahn, ChemPhysChem, 2011, **12**, 3274-3280.
59. P. E. M. Siegbahn, Phys. Chem. Chem. Phys, 2012, **14**, 4849-4856.
60. S. Luber, I. Rivalta, Y. Umeya, K. Kawakami, J. R. Shen, N. Kamiya, G. R. Brudvig and V. S. Batsita, Biochemistry, 2011, **50**, 6308–6311.
61. I. Rivalta, G. R. Brudvig and V. S. Batsita, Curr. Opin. Chem. Biol., 2012, **16**, 11–18.
62. A. Robertazzi, A. Galstyan and E. W. Knapp, CrystEngComm, 2011, **13**, 6369–6372.
63. A. Galstyan, A. Robertazzi and E. W. Knapp, J. Am. Chem.Soc., 2012, **134**, 7442–7449.
64. S. Petrie, R. Stranger and R. J. Pace, Angew. Chem., Int. Ed., 2010, **49**, 4233–4236.
65. S. Petrie, P. Gatt, R. Stranger and R. J. Pace, Phys. Chem. Chem. Phys., 2012, **14**, 4651–4657.
66. S. Petrie, P. Gatt, R. Stranger and R. J. Pace, Phys. Chem. Chem. Phys., 2012, **14**, 11333–11343.
67. P. Gatt, S. Petrie, R. Stranger and R. J. Pace, 2012, **51**, 12025–12028.
68. R. G. Parr and Y. Yang, Density Functional Theory of Atoms and Molecules, Oxford University Press, Inc., 1989.
69. A. J. Becke, J. Chem. Phys., 1993, **98**, 5648-5653.
70. E. Davidson and D. Feller, Chem. Rev., 1986, **86**, 681–696.
71. M. J. Frisch, et al., Gaussian 09, Revision, A.1., Gaussian, Inc., Wallingford, CT, 2009.
72. M. Shoji, Y. Nishiyama, Y. Maruno, K. Koizumi, Y. Kitagawa, S. Yamanaka, T. Kawakami, M. Okumura, K. Yamaguchi, Int. J. Quant. Chem. 2004, **100,** 887-906.
73. H. Isobe, M. Shoji, K. Koizumi, Y. Kitagawa, S. Yamanaka, S. Kuramitsu and K. Yamaguchi, Polyhedron 2005, **24**, 2767-2773.
74. S. Mukherjee, J. A. Stull, J. Yano, T. C. Stamatatos, K. Pringouri, T. A. Stich, K. A. Abboud, R. D. Britt, V. K. Yachandra and G. Christou, Proc. Natl. Acad. Sci. U. S. A. 2012, **109**, 2257–2262.

75. A. Zouni, H. T. Witt, J. Kern, P. Fromme, N. Krauss, W. Saenger, P. Orth, Nature, 2001, **409**, 739-743.
76. N. Kamiya, J. R. Shen, Proc. Natl. Acad. Sci. USA 2003, **100**, 98-103.
77. K. Ferreira, T. Iverson, K. Maghlaoui, J. Baber, S. Iwata, Science, 2004, **303** 1831-1838.
78. J. Biesiadka, B. Loll, J. Kern, K. D. Irrgang, A. Zouni, Phys. Chem. Chem. Phys. , 2004, **6** , 4733-4736.
79. B. Loll, J. Kern, W. Saenger, A. Zouni, J. Biesiadka, Nature, 2005, **438**, 1040-1044.
80. R. Krivanek, J. Kern, A. Zouni, H. Dau, M. Haumann, Biochim. Biophys. Acta, 2007, **1767**, 520-527.
81. A. Guskov, J. Kern, A. Gabdulkhakov, M. Broser, A. Zouni, W. Saenger, Nature strutural & molecular biology, 2009, **16**, 334-342.
82. K. Kawakami, Y. Umena, N. Kamiya, J. R. Shen, Proc. Natl. Acad. Sci. U. S. A. , 2009, **106**, 8567-8572.
83. F. H. M. Koua, Y. Umena, K. Kawakami, J. –R. Shen, Proc. Nat. Acad. Sci. 2013, **110**, 3889-3894.
84. V. K. Yachndra, K. Sauer and M. P. Klein, Chem. Rev., 1996, **96**, 2927–2950.
85. J. H. Robblee, R. M. Cinco, V. K. Yachandra, Biochim. Biophys. Acta, 2001, **1503**, 7–23.
86. R. M. Cinco, K. L. M. Holman, J. H. Robblee, J. Yano, S. A. Pizarro, E. Bellacchio, K. Sauer and V. K. Yachandra, Biochemistry, 2002, **41**, 12928–12933.
87. J. Yano, Y. Pushkar, P. Glatzel, A. Lewis, K. Sauer, J. Messinger, U. Bergmann , V. K. Yachandra, J. Am. Chem. Soc., 2005, **127**, 14974–14975.
88. J. Yano, J. Kern, K. Sauer, M. J. Latimer, Y. Pushkar, J. Biesiadka, B. Loll, W. Saenger, J. Messinger, A. Zouni, V. K. Yachandra, Science, 2006, **314**, 821–825.
89. G. Glockner, J. Kern, M. Broser, A. Zouni, V. Yachandra, J. Yano, J. Biol. Chem. doi: 10.1074/jbc.M113.476622.
90. J. P. McEvoy, G. W. Brudvig, Phys. Chem. Chem. Phys. 2004, **6**, 4754-4763.
91. J. M. Baber, Phil, Trans. Roy. Soc. 2008, **1504**, 2665-2674.
92. K. Yamaguchi, M. Shoji, T. Saito, H. Isobe, S. Nishihara, K. Koizumi, S. Yamada, T. Kawakami, Y. Kitagawa, S. Yamanaka, M. Okumura, Int. J. Quant. Chem. 2010, **110**, 3101-3128

Legends of figures

Figure 1 (A) right (R)-opened structure $S_{1a}(R)(X=O;Y=H_2O)$ in the S_1 state of oxygen evolving complex (OEC) of photosystem II (PSII); (B) proton-shifted structure $S_{1b}(C)(X=Y=OH)$; (C) right (R)-opened water-inserted structure $S_{3a}(R)(X=O;Y=H_2O, W=OH)$ in the S_3 state and (D) left (R)-opened water-inserted structure $S_{3a}(L)(X=O;Y=H_2O, W=OH)$ in the S_3 state.

Figure 2 Energy levels of the eight different spin configurations of the right-opend structure $\mathbf{S_{1a}}(R)(X=O;Y=H_2O)$ in the S_1 state of OEC of PSII by the UB3LYP calculations under three different procedures: (A) vertical approximation for which the full geometry optimized structure for the highest spin state is assumed for other seven configurations; (B) adiabatic approximation where full geometry optimizations of all the spin configurations are performed; (C) adiabatic plus zero point energy (ZPE) corrections are performed. The triplet (S=1) configuration (↑↓↓↑) was the ground state for $\mathbf{S_{1a}}(R)$.

Figure 3 Energy levels of the eight different spin configurations of the proton-shifted structure $\mathbf{S_{1b}}(C)(X=O;Y=H_2O)$ in the S_1 state of OEC of PSII by the UB3LYP calculations under three different procedures: (A) vertical approximation for which the full geometry optimized structure for the highest spin state is assumed for other seven configurations; (B) adiabatic approximation where full geometry optimizations of all the spin configurations are performed; (C) adiabatic plus zero point energy (ZPE) corrections are performed. The triplet (S=1) configuration (↑↓↑↓) was the ground state for $\mathbf{S_{1b}}(C)$.

Figure 4 Excitation energies of the right-opend structure $\mathbf{S_{1a}}(R)(X=O;Y=H_2O)$ in the S_1 state of OEC of PSII by the exact diagonalization of the spin Hamiltonian matrix consisted of the J values determined by three different procedures: (A) vertical approximation for which the full geometry optimized structure for the highest spin state is assumed for other seven configurations; (B) adiabatic approximation where full geometry optimizations of all the spin configurations are performed; (C) adiabatic plus zero point energy (ZPE) corrections are performed. The triplet (S=1) state was the ground state by

the (A) and (B) procedures, whereas the singlet state (S=0) was the ground state by the (C) procedure.

Figure 5 Energy levels of the eight different spin configurations of the right-opened water-inserted structure $\mathbf{S_{3a}}$(R)(X=O;Y=H_2O,Z=OH) in the S_3 state of OEC of PSII by the UB3LYP calculations under three different procedures: (A) vertical approximation for which the full geometry optimized structure for the highest spin state is assumed for other seven configurations; (B) adiabatic approximation where full geometry optimizations of all the spin configurations are performed; (C) adiabatic plus zero point energy (ZPE) corrections are performed. The singlet (S=0) configuration (↑↓↓↑) was the ground state for $\mathbf{S_{3a}}$(R).

Figure 6 Energy levels of the eight different spin configurations of the left-opened water-inserted structure $\mathbf{S_{3a}}$(L)(X=O;Y=H_2O,Z=OH) in the S_3 state of OEC of PSII by the UB3LYP calculations under three different procedures: (A) vertical approximation for which the full geometry optimized structure for the highest spin state is assumed for other seven configurations; (B) adiabatic approximation where full geometry optimizations of all the spin configurations are performed; (C) adiabatic plus zero point energy (ZPE) corrections are performed. The septet (S=5/2) configuration (↓↑↑↑) was the ground state for $\mathbf{S_{3a}}$(L).

Figure 7 Excitation energies of the right-opend structure $\mathbf{S_{3a}}$(L)(X=O;Y=H_2O, W=OH) in the S_3 state of OEC of PSII by the exact diagonalization of the spin Hamiltonian matrix consisted of the J values determined by three different procedures: vertical approximation for which the full geometry optimized structure for the highest spin state is assumed for other seven configurations; (B) adiabatic approximation where full geometry optimizations of all the spin configurations are performed; (C) adiabatic plus zero point energy (ZPE) corrections are performed. The singlet (S=5/2) state was the ground state for $\mathbf{S_{3a}}$(L) by all the procedures.

Figure 8 (A) hydroxyl-radical coupled right (R)-opened structure S_{2a}(R)(X=O; Z= H_2O)-OH• (Mn_a) in the S_3 state of OEC of PSII; (B) hydroxyl-radical coupled right (R)-opened structure S_{2a}(R)(X=O; Y=H_2O) in the S_3 state; (C) oxyl-radical coupled left (L)-opened structure S_{2a}(R)(X=O; Y= H_2O)-O• ($Mn(III)_a$) in the S_3 state of OEC of PSII; (D) oxyl-radical coupled right (R)-opened structure S_{2a}(R)(X=O; Y= H_2O)-O• ($Mn(III)_d$) in the S_3 state; (E) oxyl-radical coupled left (L)-opened structure S_{2a}(L)'(X=O•; Y= H_2O)-O• ($Mn(IV)_a$) in the S_4 state; (F) oxyl-radical coupled right (R)-opened structure S_{2a}(R)'(X=O•; Y= H_2O)-O• ($Mn(IV)_d$) in the S_4 state. The spin configurations are schematically expressed by the up(↑)- and down(↓) spins.

Table 1. The effective exchange integrals[a] (cm^{-1}) of the Heisenberg spin Hamiltonian model for the right-opened structure, S_{1a}(R), in the S_1 state of the Kok cycle for OEC of PSII

J	$\mathbf{S_{1a}}$(R)[1,a)]	$\mathbf{S_{1a}}$(R)[2,a)]	$\mathbf{S_{1a}}$(R)[1,b)]	$\mathbf{S_{1a}}$(R)[2,b)]	$\mathbf{S_{1a}}$(R)[1,c)]	$\mathbf{S_{1a}}$(R)[2,c)]
J_{ab}	-69.9	-69.4	-77.7	-77.1	-76.6	-75.5
J_{ac}	2.77	2.55	2.91	2.91	2.48	3.06
J_{ad}	0.55	0.38	0.44	0.11	0.33	-0.33
J_{bc}	20.4	20.1	19.0	18.4	15.5	14.4
J_{bd}	10.6	7.79	9.61	6.84	7.42	4.95
J_{cd}	-33.8	-33.5	-36.1	-35.6	-36.8	-35.9

[1)]Analytical eq. was used. [2)] Generalized approximate spin projection (GAP). [a)] Vertical energy levels are used. [b)] Adiabatic energy levels are used. [c)]Adiabatic energy levels + zero-point-energy (ZPE) corrections are used.

Table 2. The effective exchange integrals[a] (cm^{-1}) of the Heisenberg spin Hamiltonian model for the proton-shifted structure, $S_{1b}(C)$, in the S1 state of the Kok cycle for OEC of PSII

J	$\mathbf{S_{1b}}(C)^{1,a)}$	$\mathbf{S_{1b}}(C)^{2,a)}$	$\mathbf{S_{1b}}(C)^{1,b)}$	$\mathbf{S_{1b}}(C)^{2,b)}$	$\mathbf{S_{1b}}(C)^{1,c)}$	$\mathbf{S_{1b}}(C)^{2,c)}$
J_{ab}	-4.51	-4.29	-7.86	-8.14	-8.50	-8.50
J_{ac}	0.73	0.51	0.15	0.44	-0.29	0.51
J_{ad}	-3.93	-4.10	-4.26	-4.04	-4.04	-3.88
J_{bc}	6.21	5.92	3.88	4.27	2.52	2.81
J_{bd}	-1.02	-1.24	-2.33	-2.04	-2.33	-2.11
J_{cd}	-34.8	-34.5	-36.3	-36.5	-37.4	-37.6

[1)]Analytical eq. is used. [2)] Generalized approximate spin projection (GAP). [a)] Vertical energy levels are used. [b)] Adiabatic energy levels are used. [c)]Adiabatic energy levels + zero-point-energy (ZPE) corrections are used.

Table 3. The excitation energies and projection factors obtained for the $S_{1a}(R)$ by the exact diagonalyzation of the spin Hamiltonian model

Methods	Energy(cm^{-})	$\mathbf{Mn(III)_a}$	$\mathbf{Mn(IV)_b}$	$\mathbf{Mn(IV)_c}$	$\mathbf{Mn(III)_d}$
$V(G,S=1)^{1,a)}$	0.00	0.87	-0.51	-0.64	1.15
$V(1^{th},S=0)^{1,b)}$	1.59	0.00	0.00	0.00	0.00
$V(2^{th},S=1)^{1,c)}$	79.2	-0.64	0.43	0.37	0.84
$A(G,S=1)^{2,a)}$	0.00	0.99	-0.51	-0.61	1.13
$A(1^{th},S=0)^{2,b)}$	0.14	0.00	0.00	0.00	0.00
$A(2^{th},S=1)^{2,c)}$	86.6	-0.63	0.40	0.36	0.87
$ZPE(G,S=0)^{3,a)}$	0.00	0.00	0.00	0.00	0.00
$ZPE(2^{th},S=1)^{3,b)}$	2.88	1.00	-0.51	-0.57	1.08
$ZPE(3^{th},S=1)^{3,c)}$	92.9	-0.62	0.38	0.32	0.92

[1)]Vertical, [2)]Adiabatic, [3)]Adiabatic + ZPE, [a)]Ground (G) state, [b)]First excited state, [c)] Second excited state,

Table 4. The effective exchange integrals[a] (cm^{-1}) of the Heisenberg spin Hamiltonian model for the right-opened structure, $S_{3a}(R)$-H_2O, in the S_3 state of the Kok cycle for OEC of PSII

J	$\mathbf{S_{3a}}(R)^{1,a)}$	$\mathbf{S_{3a}}(R)^{2,a)}$	$\mathbf{S_{3a}}(R)^{1,b)}$	$\mathbf{S_{3a}}(R)^{2,b)}$	$\mathbf{S_{3a}}(R)^{1,c)}$	$\mathbf{S_{3a}}(R)^{2,c)}$
J_{ab}	-17.3	-17.1	-23.7	-23.7	-25.4	-25.4
J_{ac}	0.39	0.29	0.00	0.10	0.39	0.39
J_{ad}	4.08	3.98	3.88	3.98	4.08	4.08
J_{bc}	8.93	8.82	6.41	6.49	5.24	5.23
J_{bd}	-2.52	-2.62	-3.30	-3.20	-3.88	-3.88
J_{cd}	0.78	0.87	-2.91	-3.00	-4.47	-4.46

[1)]Analytical eq. is used. [2)] Generalized approximate spin projection (GAP). [a)] Vertical energy levels are used. [b)] Adiabatic energy levels are used. [c)]Adiabatic energy levels + zero-point-energy (ZPE) corrections are used.

Table 5. The effective exchange integrals[a] (cm^{-1}) of the Heisenberg spin Hamiltonian model for the left-opened structure, $S_{3a}(L)$-H_20, in the S_3 state of the Kok cycle for OEC of PSII

J	$\mathbf{S_{3a}}(L)^{1,a)}$	$\mathbf{S_{3a}}(L)^{2,a)}$	$\mathbf{S_{3a}}(L)^{1,b)}$	$\mathbf{S_{3a}}(L)^{2,b)}$	$\mathbf{S_{3a}}(L)^{1,c)}$	$\mathbf{S_{3a}}(L)^{2,c)}$
J_{ab}	-22.7	-22.1	-36.7	-36.2	-31.1	-30.7
J_{ac}	2.52	2.04	2.14	1.85	1.94	1.75
J_{ad}	5.44	4.95	5.82	5.54	5.44	5.25
J_{bc}	43.3	42.8	41.9	41.6	36.9	36.7
J_{bd}	-3.30	-3.59	-6.41	-6.70	-8.93	-9.12
J_{cd}	43.9	44.4	42.5	42.8	36.9	37.1

[1)]Analytical eq. is used. [2)] Generalized approximate spin projection (GAP). [a)] Vertical energy levels are used. [b)] Adiabatic energy levels are used. [c)]Adiabatic energy levels + zero-point-energy (ZPE) corrections are used.

Table 6. The excitation energies and projection factors obtained for the S_{3a}(R)-H_2O in the S_3 state by the exact diagonalyzation of the spin Hamiltonian model

Methods	Energy(cm^{-1})	**$Mn(IV)_a$**	**$Mn(IV)_b$**	**$Mn(IV)_c$**	**$Mn(IV)_d$**
V(1^{th},S=1) [1,b)]	2.47	0.06	0.06	0.44	0.44
V(2^{th},S=2) [1,b)]	8.06	0.06	0.07	0.44	0.44
V(5^{th},S=1)[1,c)]	57.4	-0.16	0.72	1.12	-0.67
A(1^{th},S=1)[2,a)]	8.22	0.12	0.02	0.44	0.42
A(2^{th},S=2)[2,b)]	25.2	0.12	0.02	0.44	0.42
A(4^{th},S=1)[2,c)]	73.8	-0.14	0.72	1.08	-0.66
ZPE(1^{th},S=1)[3,a)]	10.1	0.17	-0.03	0.46	0.40
ZPE(2^{th},S=2)[3,b)]	30.9	0.17	-0.02	0.45	0.40
ZPE(3^{th},S=3)[3,c)]	63.8	0.16	-0.02	0.45	0.41

[1)]Vertical, [2)]Adiabatic, [3)]Adiabatic + ZPE,[a)]First excited state, [b)] Second excited state, [c)] Higher excited state.

Table 7. The excitation energies and projection factors obtained for the S_{3a}(L)-H_2O in the S_3 state by the exact diagonalyzation of the spin Hamiltonian model

Methods	Energy(cm^{-1})	**$Mn(IV)_a$**	**$Mn(IV)_b$**	**$Mn(IV)_c$**	**$Mn(IV)_d$**
V(G,S=3) [1,a)]	0.00	-0.33	0.37	0.46	0.49
V(1^{th},S=4) [1,b)]	26.8	0.02	0.26	0.35	0.37
V(2^{th},S=2)[1,c)]	129	-0.41	0.25	0.63	0.53
A(G,S=3)[2,a)]	0.00	-0.28	0.32	0.47	0.50
A(1^{th},S=4)[2,b)]	50.1	0.05	0.22	0.36	0.38
A(2^{th},S=2)[2,c)]	119	-0.34	0.18	0.62	0.54
ZPE(G,S=3)[3,a)]	0.00	-0.25	0.28	0.46	0.50
ZPE(1^{th},S=4)[3,c)]	39.1	0.06	0.20	0.36	0.37
ZPE(2^{th},S=2)[3,d)]	84.3	-0.31	0.15	0.61	0.55

[1)]Vertical, [2)]Adiabatic, [3)]Adiabatic + ZPE, [a)]Ground state, [b)]First excited state, [c)] Second excited state,[d)] Higher excited state.

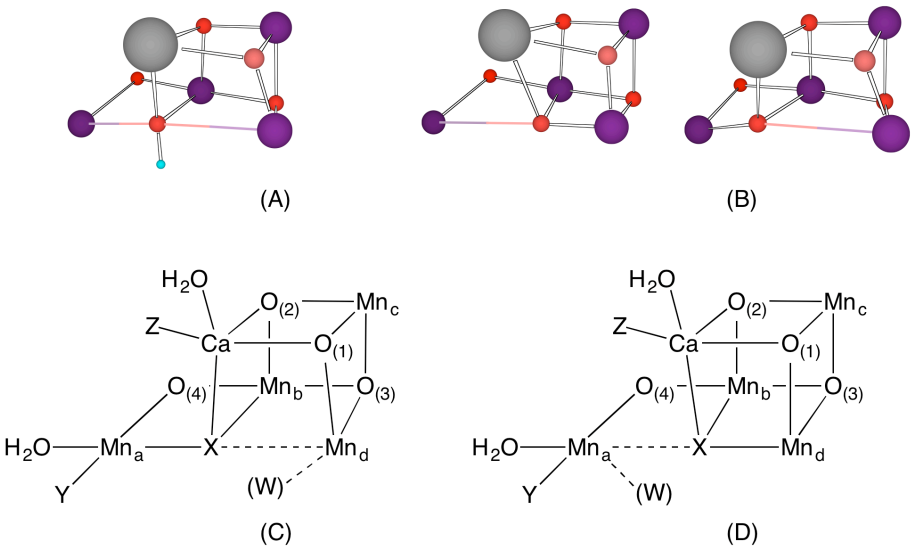

Fig. 1

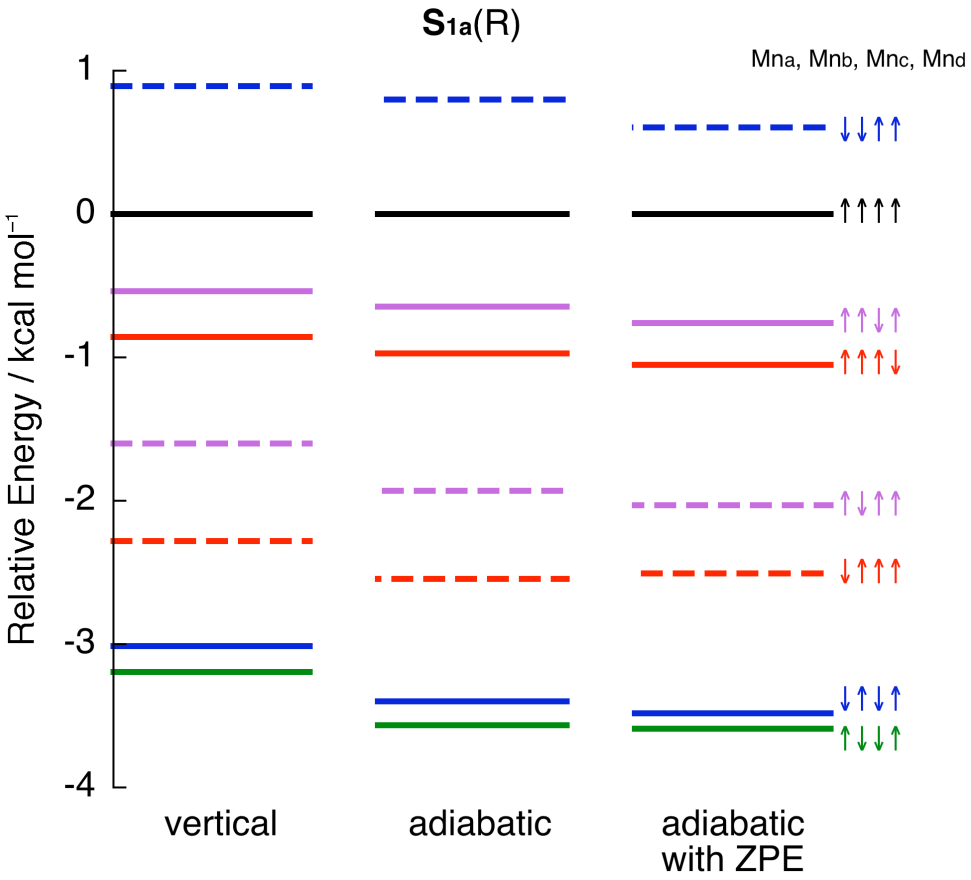

Figure 2

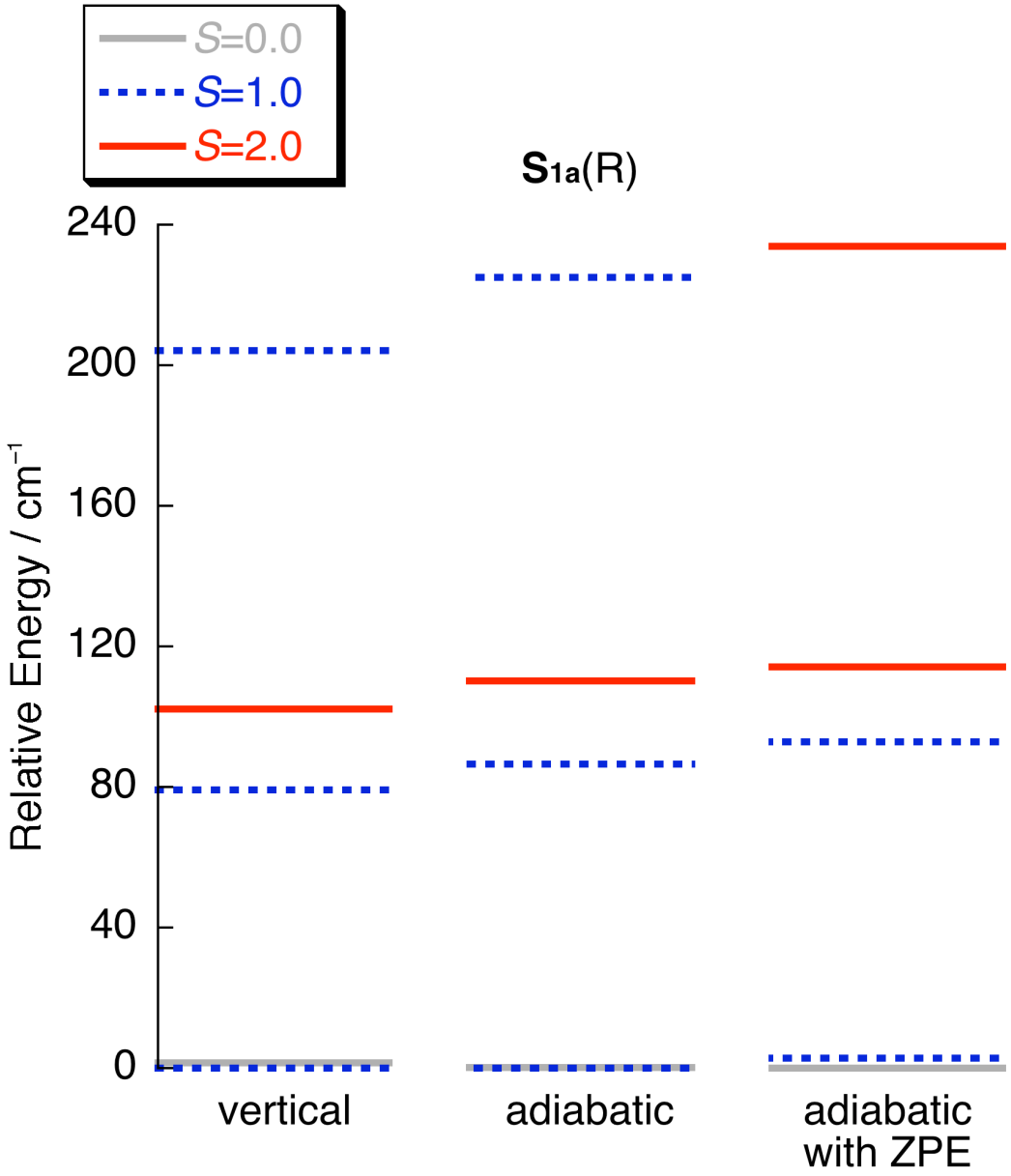

Fig.3

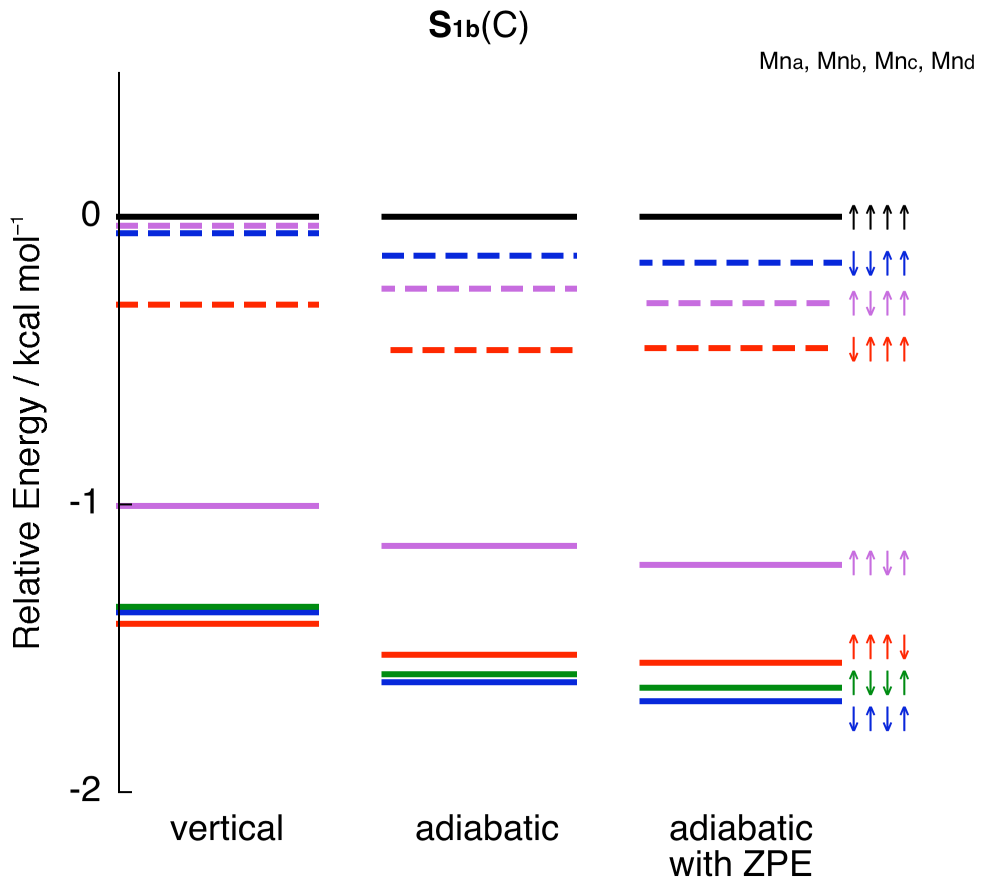

Figure 4

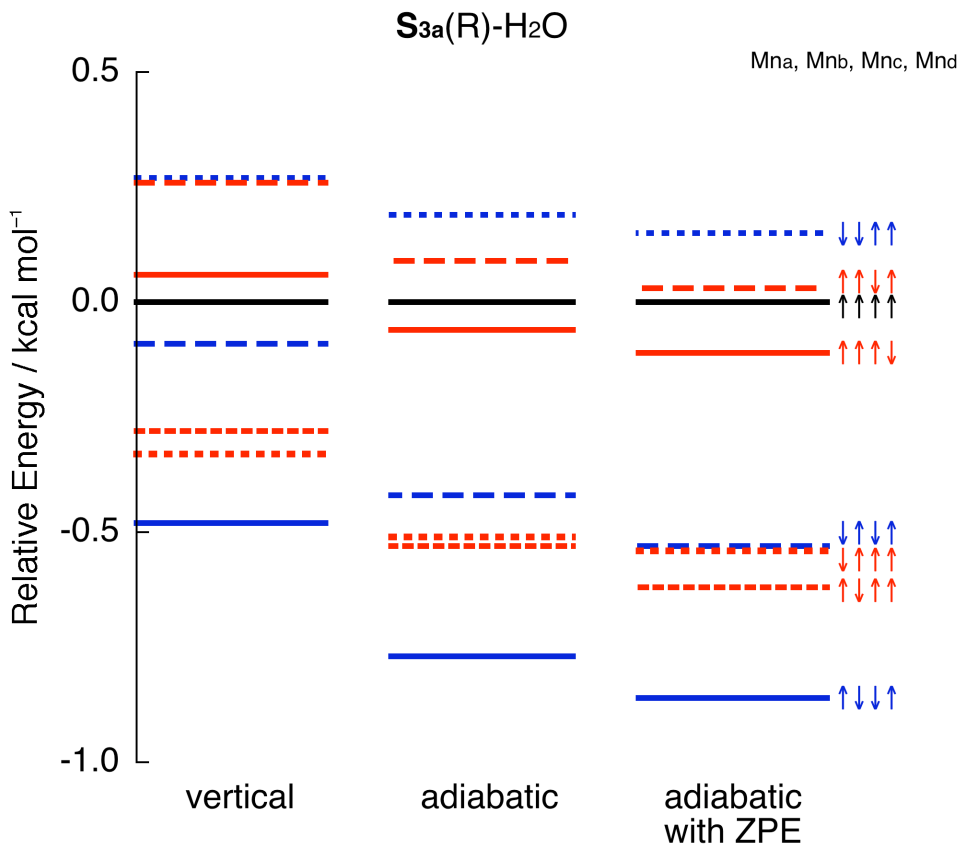

Figure 5

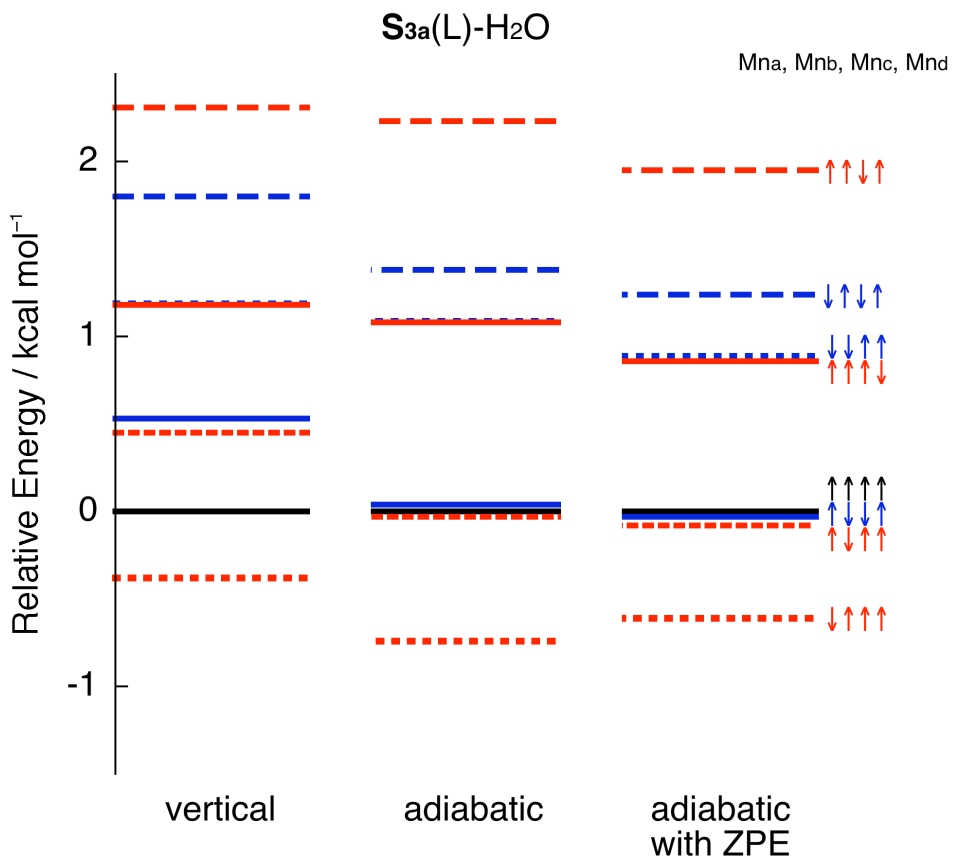

Figure 6

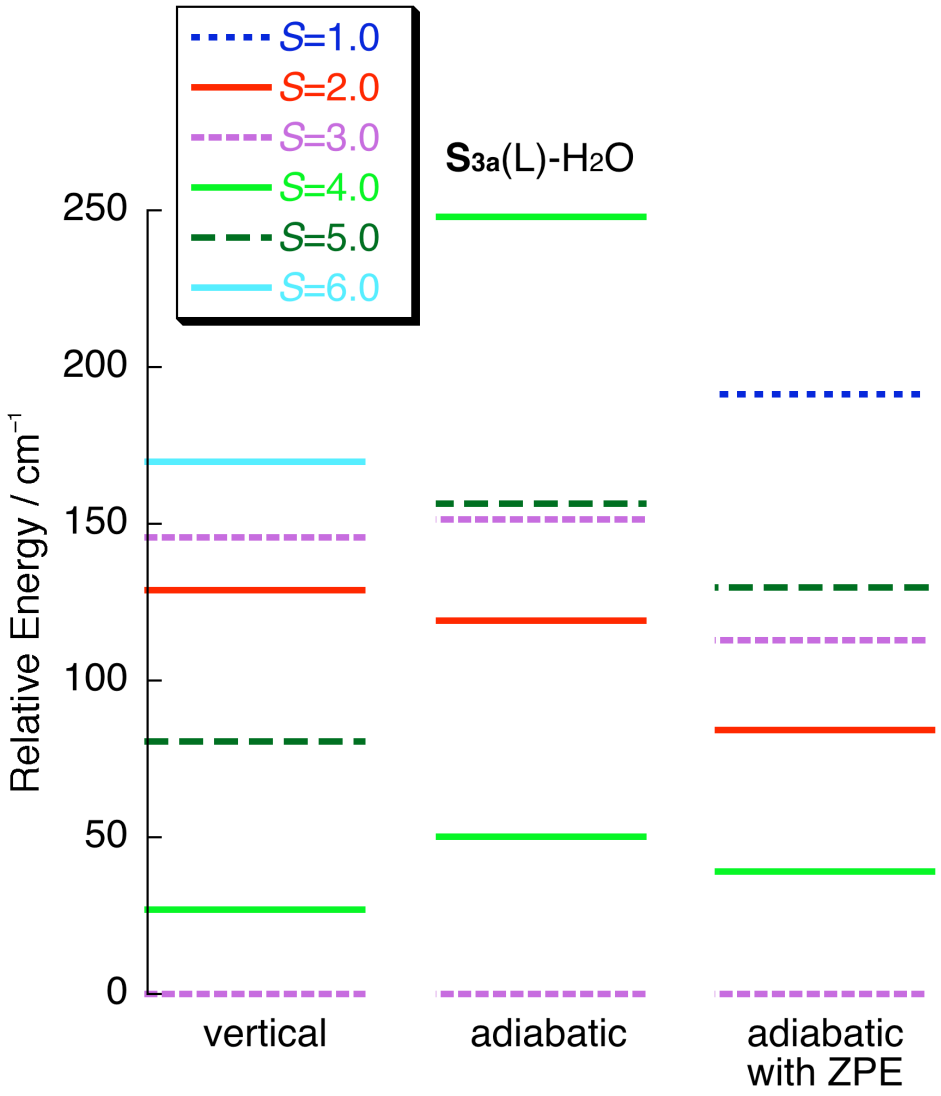

Figure 7

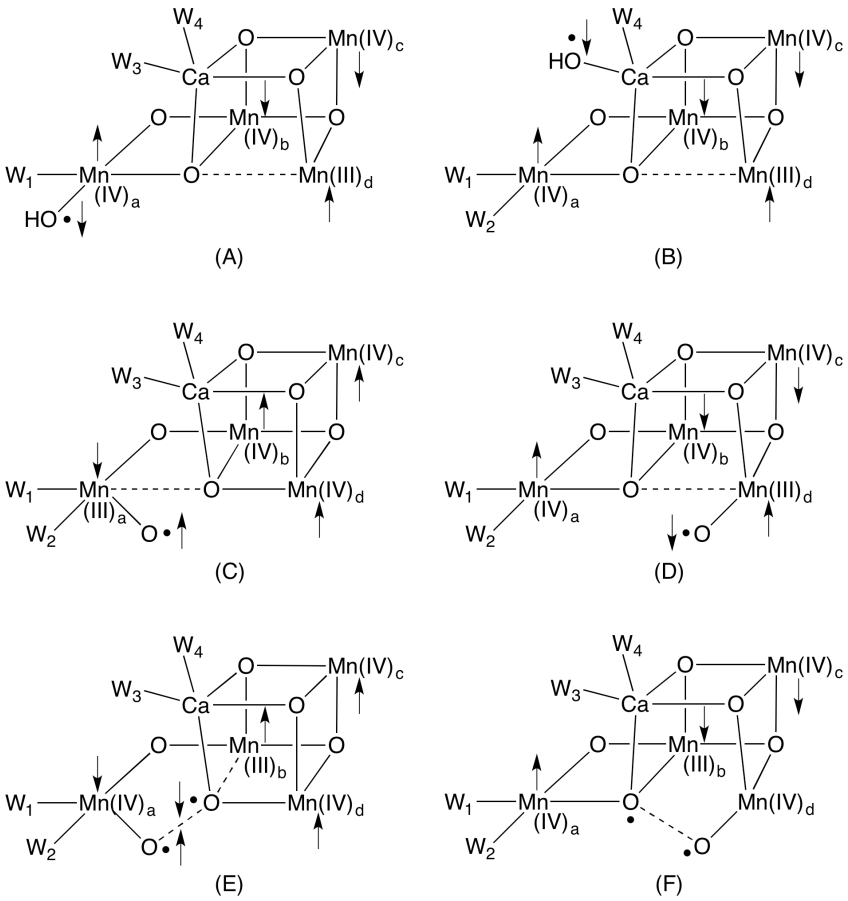

Figure 8